Magnetically Modified Single and Turbostratic Stacked Graphenes from Tris(2,2'-bipyridyl) Iron(II) Ion-Exchanged Graphite Oxide

ARTICLE *in* THE JOURNAL OF PHYSICAL CHEMISTRY B · SEPTEMBER 2008

Impact Factor: 3.3 · DOI: 10.1021/jp802879a · Source: PubMed

THE JOURNAL OF PHYSICAL CHEMISTRY B

Article

Magnetically Modified Single and Turbostratic Stacked Graphenes from Tris(2,2#-bipyridyl) Iron(II) Ion-Exchanged Graphite Oxide

Tama#s Szabo#, Aristides Bakandritsos, Vassilis Tzitzios, Eamonn Devlin, Dimitris Petridis, and Imre De#ka#ny

J. Phys. Chem. B, **2008**, 112 (46), 14461-14469 • DOI: 10.1021/jp802879a • Publication Date (Web): 05 August 2008

Magnetically Modified Single and Turbostratic Stacked Graphenes from Tris(2,2′-bipyridyl) Iron(II) Ion-Exchanged Graphite Oxide†

Tamás Szabó,‡ Aristides Bakandritsos,§,|| Vassilis Tzitzios,§ Eamonn Devlin,§ Dimitris Petridis,§ and Imre Dékány*,‡,⊥

Department of Colloid Chemistry and Supramolecular and Nanostructured Materials Research Group of the Hungarian Academy of Sciences, University of Szeged, Aradi vértanúk tere 1, H-6720 Szeged, Hungary, Materials Science Department, University of Patras, Rio 26504, Patra, Greece, and Institute of Materials Science, NCSR "DEMOKRITOS", GR-15310 Athens, Greece

Received: April 3, 2008; Revised Manuscript Received: June 9, 2008

Loading of graphite oxide (GO) with tris(2,2′-bipyridyl) iron(II) ions and subsequent calcination affords a novel graphene-based composite with magnetic and electrically conductive properties. The pH of the starting aqueous suspension and the washing procedure play a crucial role in the successful immobilization of the iron precursor, which is mainly governed by ion exchange. The complex is intercalated between the graphene oxide layers, where it adopts a distorted conformation. Rapid heating of this solid results in the deflagration of GO and the formation of ultrafine ($d = 2-14$ nm) Fe_2O_3 particles with maghemite as the dominant phase. The superparamagnetic maghemite crystals are dispersed uniformly in the high-surface-area diamagnetic matrix built up from single or turbostratic stacked graphenes.

Introduction

The benefits of ultrafine magnetic nanocrystals are increasingly realized and exploited. Such nanoparticles with sizes approaching that of a single magnetic domain possess important applications in catalysis,[1] biomedicine,[2] or magnetic data storage.[3] For many of these purposes, immobilization of magnetic iron oxides on solid supports is of great importance. Various inorganic colloids (clays,[4–6] silica,[7,8] and zeolites[9]) can be decorated with magnetic γ-Fe_2O_3 (maghemite) or magnetite (Fe_3O_4) nanoparticles. γ-Fe_2O_3 impregnated carbon nanotubes (CNTs) have also been fabricated.[10] However, there are very few reports on the preparation of iron oxide/graphite nanocomposites by simple wet-chemical methods.[11–13] These solution-based techniques cannot be readily applied on graphite because the cleavage of coarse graphite crystallites along their *c*-axes to nanometric graphene lamellae is not possible by the usual physical or soft chemical methods. Graphenes form atomically thin carbon layers, and carbon nanotubes can be derived from their rolling up. However, they seem equally or more competitive for future nanoelectronics in terms of production cost while their strength and electric conductivity is similar to the CNTs.[14]

Until recently, there were no efficient approaches to produce bulky amounts of processable graphene sheets, although it was observed by Boehm et al. in their early electron microscopic study that reduced graphite oxide (GO) afforded very thin particles with thicknesses of several or probably only one elementary carbon layer.[15] The renewable interest in graphite oxide substantiated that single graphene sheets can be produced in large scale by the thermal expansion or chemical reduction of this compound.[16–20] GO possesses other excellent physicochemical properties that make it a feasible starting material for the preparation of exfoliated or intercalated nanocomposites.[21–27] The lamellar surfaces of GO are polar owing to the oxygenated functional groups attached to the carbon grid.[28,29] Adsorption of ammonia on air-dry GO[30,31] and the relatively low pH of aqueous GO suspensions[32] show that a considerable part of these surface sites is acidic. Therefore, this covalent graphite compound may be considered as hydrophilic and acidic graphite. The higher basal spacing (0.6 nm) of GO as compared to graphite (0.334 nm), together with the electrostatic repulsion between the charged surface sites results in weak interlayer interactions. The reduced adhesion of the graphene oxides makes the delamination of GO particles to quasi-2D carbonaceous sheets very easy in dilute alkaline suspensions,[32] rendering GO highly advantageous for nanofabrication.[33–36]

In the present paper, we report on the preparation of a novel magnetic and electrically conductive derivative of high-surface-area graphitic nanoplatelets from graphite oxide and tris(2,2′-bipyridyl) iron(II) sulfate. The latter acts as the precursor of magnetic Fe_2O_3 particles, while the decomposition of GO provides the conductive matrix for these particles. The mechanism and criteria of the formation of the iron oxide/carbon composites are discussed together with their physicochemical characterization.

Experimental Section

Materials. The host graphite was a synthetic specimen from Aldrich (particle size <20 μm). $NaClO_3$ (Aldrich), fuming HNO_3 (Fluka), HCl (Reanal), iron(II) ammonium sulfate (Merck), 2,2′-bipyridine, and NaOH (Panreac) were analytical grade chemicals.

Synthesis of Graphite Oxide. GO was prepared by the Brodie method.[37] (*CAUTION: This procedure is very dangerous due to possible deflagration of the reaction mixture!*) A 10 g portion of graphite and 85 g of $NaClO_3$ were mixed in a round

† Part of the "Janos H. Fendler Memorial Issue".

* Author to whom correspondence should be addressed. Phone: +36-62-544210. Fax: +36-62-544042. E-mail: i.dekany@chem.u-szeged.hu.
‡ Department of Colloid Chemistry, University of Szeged.
§ NCSR "DEMOKRITOS".
|| University of Patras.
⊥ Supramolecular and Nanostructured Materials Research Group of the Hungarian Academy of Sciences, University of Szeged.

10.1021/jp802879a CCC: $40.75
Published on Web 08/05/2008

flask placed into an ice bath. A total of 60 mL of fuming HNO_3 was added from a dropping funnel in 210 min during periodic stirring. The thick slurry was then left aging for 18 h at room temperature. The loss of large quantities of nitrous fumes was prevented by a distillation column and the addition of an extra volume of acid (40 mL) after aging. Next, it was slowly (<1.5 °C/min) heated to 60 °C by a basket heater and kept at 60 ± 1 °C for 8 h. The solid GO sample was washed with 5 × 200 mL of 3 M HCl solution and 7 × 1 L of distilled water to remove acidic and saline impurities until the electrical conductivity of the supernatant was below 10 μS/cm. Finally, the suspension was filtered and dried at 60 °C to yield a brown graphite oxide with an elemental composition of $C_2O_{0.75}H_{0.24}$ and a water content of 10.0 wt % at 24 °C and 46% relative humidity.

Preparation of the Magnetic Iron Oxide/Graphitic Carbon Composites. The nanocomposites were produced in a two-step process. In the first step, the iron precursor was inserted in the GO structure by ion exchange as follows: 200 mg of GO was dispersed in 400 mL of distilled water, sonicated for 10 min, and left stirring for 1−2 h. 0.4 mmol $(NH_4)_2Fe(SO_4)_2 \times 6\ H_2O$ (Mohr's salt) was dissolved in 100 mL of water, and 1.2 mmol of 2,2′-bipyridine was added for the stoichiometric formation of tris-bypiridine iron(II) complexes, which will be abbreviated as $Fe(bpy)_3^{2+}$. Next, the ruby red solution of the complex was poured in the GO suspension under intensive stirring and left so for 3 days. The suspension was then centrifuged at 3500 rpm for 5 min, and the compact sediment obtained is denoted as GOFe4 ("4" refers to the final pH value of the suspension). The excess $Fe(bpy)_3^{2+}$, which was present in the supernatant and in the pores of the wet sediment, was removed by washing with distilled water, sonication, and centrifugation until the supernatant became transparent. The final sediment was spread over glass and dried at room temperature.

The ion-exchange reaction was repeated under slightly alkaline conditions. In this case, 1 M NaOH was added to the GO suspension until it reached pH 9. The pH of the $Fe(bpy)_3SO_4$ solution was also set to 9. After mixing, an instant flocculation was observed and the formed flocs constituted a voluminous and soft sediment (denoted as GOFe9) after centrifugation. These are in stark contrast with the GOFe4 system where no flocculation was observed during the reaction and the sediment volume was as low as that for pure GO. Another difference was that GOFe9 could not be washed with water to get a clear supernatant in 3−4 steps. Apparently, the red $Fe(bpy)_3^{2+}$ was gradually leaching out from the solid upon the successive (at least up to 8) washing procedures. However, it was found that significant leaching could be avoided by using a dilute NaOH solution (pH 9) as a washing medium instead of water (pH 6).

In the second step, the ion-exchanged GO solids were subjected to heat treatment at 350 °C in air atmosphere. For experiments with low heating rate (20 °C/min), samples were loaded and kept for 30 min at the calcination temperature in a ceramic crucible loosely covered by Al foil. This enables contact with the atmosphere but the voluminous, fluffy carbon soot formed by the fast decomposition (deflagration) of GO is retained in the vessel. The iron loaded graphite oxides were calcined also with high heating rate. In this case, a thin test tube was loaded with ca. 20 mg of solid and put in a furnace preheated to 350 °C. The GO was instantly blown up and the sample was collected after calcination for 5 min. The obtained carbon supported iron oxide specimens are code-named as CFe4-sl, CFe4-rap, CFe9-sl, and CFe9-rap, where the numbers refer to the pH of the ion-exchange reaction while "sl" and "rap" correspond to the slow or rapid heat treatment, respectively. For comparison, pure GO was also rapidly heated to 350 °C to obtain pure turbostratic carbon (denoted as "GO soot").

Characterization Techniques. The iron content of the samples was determined by inductively coupled plasma atomic emission spectroscopy, using a sequential all-argon Jobin Yvon 24 type spectrometer. For each sample, three parallel determinations were performed at the 238.2 nm emission wavelength.

The pH-dependent surface charge of the present graphite oxide sample was determined by potentiometric acid−base titration under a CO_2-free atmosphere using 0.1 M NaOH as titrant and NaCl as background electrolyte in 5 mM concentration. The detailed description of the procedure and the evaluation of the surface charging curve can be found in our earlier publication.[32]

XRD measurements were performed on a Bruker D8 Advance diffractometer operating with a Cu anode (40 kV, 30 mA) in parallel beam geometry using a PGM2 Göbel mirror.

Thermal analyses were done with a Mettler Toledo TGA/SDTA 851^e instrument controlled by the Mettler Star^e 8.10 program. Measurements were performed on 2−10 mg solids with a heating rate of 5 °C/min in air atmosphere.

Samples for transmission electron microscopy (TEM) were prepared by casting a droplet of a dilute, aqueous suspension of the GOFe or CFe solids on copper grids coated by Formvar film. Micrographs were obtained by a CM-10 electron microscope (operating at 100 kV accelerating voltage) equipped with a side-mounted CCD camera "Mega View II" (Soft Imaging System Co.). The size distribution of the particles was determined by using UTSCSA Image Tool 3 software after counting at least 120 particles.

N_2 adsorption isotherms of the samples kept previously in a vacuum at 50 °C for 12 h were determined at 77 K in a Micromeritics Gemini 2375 automated sorptometer.

For small-angle X-ray scattering (SAXS) investigations, Cu Kα X-radiation was generated in a Philips PW 1830 source. The primary beam of 20 mm width and 80 μm thickness was directed through a Ni filter into an evacuated KCEC/3 type compact Kratky camera where it scattered on the powdered composites fixed in a 0.5 mm thick Cu or 1 mm thick Al sample holder perpendicular to the beam. The intensity of the scattered radiation was measured by a MBraun PSD 50 M type position sensitive X-ray detector having 1024 channels in the 2θ range of 0.05−7°. The absolute values of scattering intensities of the samples, determined by the moving slit method, were normalized and corrected with that of the background.

The density of the samples used for SAXS calculations was measured by a helium pycnometer (Micromeritics 1305).

Magnetic measurements were carried out at room temperature with a vibrating sample magnetometer (VSM).

Electric conductivity measurements were performed by a Keithley 2400 source meter at room temperature in a two-wire direct current configuration.

Results

XRD Analysis of GOFe Samples. Figure 1 shows the X-ray diffractograms of GO and the $Fe(bpy)_3^{2+}$-exchanged solids, while the XRD parameters are found in Table 1. The patterns of GO and GOFe4 samples are very similar and feature a single reflection, which originates from the diffraction on the (002) layer planes of the oxidized graphenes. The basal spacing of GO is 0.66 nm. It increases by 0.04 nm for GOFe4, which simply reflects a slight change in the hydration state of the GO surfaces.[38] The diffractograms of GOFe9 samples show more pronounced differences from GO. First, the (002) reflections

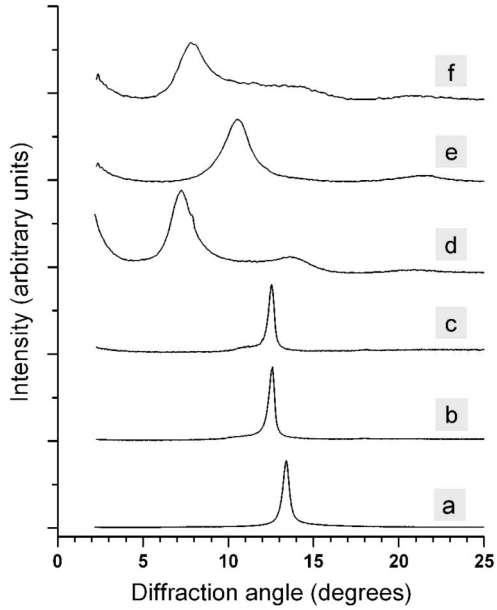

Figure 1. XRD patterns of GO (a), GOFe4 unwashed (b), GOFe4 washed with water (c), GOFe9 unwashed (d), GOFe9 washed with water (e), and GOFe9 washed with NaOH solution of pH 9 (f).

TABLE 1: XRD Parameters, Iron Contents, Deflagration Temperatures, and Specific Surface Areas of Pristine and Ion-Exchanged GO Derivatives

sample	2Θ°	d_{002} (nm)	L_c (nm)	N	Fe content (wt %)	τ (°C)	a^S_{BET} (m^2/g)
GO	13.40	0.661	22	33	0.0	275	11
GOFe4 unwash	12.60	0.703	25	36			
GOFe4 water wash	12.54	0.706	24	34	0.65	243	11
GOFe9 unwash	7.26	1.217	6.2	5			
GOFe9 water wash	10.56	0.838	5.0	6	3.40	232	
GOFe9 NaOH wash	7.92	1.116	5.8	5	3.84	217	3

shift to lower angles with c-axis repeat distances up to 1.22 nm for the unwashed sample. The interlamellar expansion is 0.56 nm as compared to the air-dry GO, which already contains water molecules between its layers. Since the thickness of an individual anhydrous graphene oxide sheet is slightly lower (0.58−0.59 nm)[39] than that of air-dry GO (0.66 nm), the real height of the interplanar spacing is 0.64 nm.

The diffraction peaks of GOFe9 samples are much broader than the sharp GO and GOFe4 reflections, which suggests a smaller particle size for samples prepared at pH 9. Indeed, the crystallite sizes (L_c) calculated from the X-ray line broadening and the mean number of GO sheets stacked along the c-axis ($N = L_c/d_{002}$) significantly decrease. As an average, 5−6 elementary GO sheets constitute an ultrafine GOFe9 particle with a thickness of only 5−6 nm. These particles have a uniform, well ordered structure as seen from the relatively high intensity of the (002) reflections and the appearance of second-order (004) reflections.

It is also apparent from Figure 1 that the d-spacing of GOFe9 abruptly decreases to 0.84 nm upon washing the GOFe9 sample with water, which suggests that large amounts of the iron precursor deintercalate. However, if the solid is washed with the dilute NaOH solution, such a significant change is not observed.

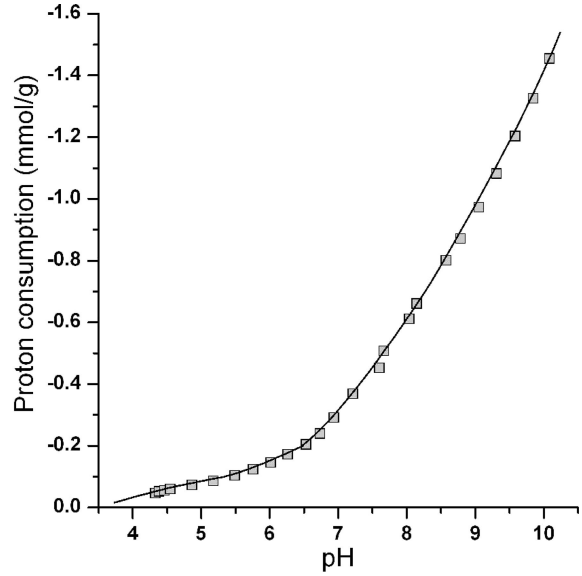

Figure 2. Surface charging curve of GO in a 1 g/L aqueous suspension, $c_{NaCl} = 5$ mM.

Iron Content of GOFe Samples. For further investigation of the adsorption/intercalation process, iron contents of the ion-exchanged graphite oxides were determined (Table 1). GOFe4 contained a very low amount of iron (0.65 wt %), while the iron content of the sample prepared at pH 9 was 6 times larger (3.84 wt %) if it was washed with a dilute NaOH solution. When GOFe9 was washed with water (pH 6), the complex was partially leached out of the solid (3.40 wt % Fe). These findings signify that the iron is more effectively immobilized on graphite oxide under slightly alkaline conditions than under the original acidic conditions.

Further information on the adsorption mechanism of $Fe(bpy)_3^{2+}$ ions can be deduced from the comparison between the adsorbed amounts of the complex and the cation-exchange capacity (CEC) of GO. The latter is not a constant value because it depends on the pH and the ionic strength of the dispersion medium. We have shown in an earlier publication that the pH-dependent surface charge (which is related to the CEC) can be characterized by acid−base titration.[32] This yields the so-called surface charging curve of GO, that gives proton consumptions of the solid as a function of the pH. Proton consumptions are equal to the amount of deprotonated (thus, negatively charged) surface functional groups of GO; therefore, they afford the actual (i.e., at a given pH and ionic strength) CEC values. The surface charging curve of the present GO sample in 5 mM NaCl is presented in Figure 2. It shows that the CEC of GO is very low at pH 4 (ca. 0.04 mmol/g). In alkaline solutions, though, the acidic (phenolic, carboxylic) groups of GO are deprotonated, which results in the progressive increase of the amount of negatively charged exchange sites. At pH 9, the CEC reaches 1 mmol/g, which is similar to that of swelling clays.

The amounts of immobilized complexes can be calculated from the iron content. These amounts are 0.14, 0.99, and 1.20 mmol/g for GOFe4, water washed GOFe9, and NaOH washed GO, respectively.

Thermal Behavior of GOFe Samples. The thermogravimetric curves of GO, GOFe4, and GOFe9 after washing with water and NaOH solution are compared in Figure 3. Three distinct weight loss steps were found for all samples. The first up to 100−120 °C is due to the loss of the water content of the samples and the slow decomposition of the thermally instable

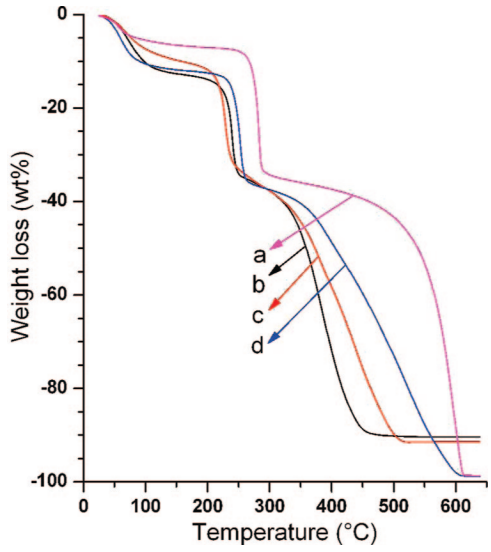

Figure 3. Thermogravimetric curves of GO (a), GOFe9 washed with water (b), GOFe9 washed with NaOH solution of pH 9 (c), and GOFe4 washed with water (d).

graphite oxide. This decomposition speeds up around 200−250 °C, after which GO reaches its deflagration point (τ). τ is defined as the temperature where the decomposition is so intense that the solid explodes to a voluminous, fluffy carbon soot. It has been recently suggested by Schniepp et al.[40] that the driving force for deflagration is the evolution of CO_2 in an exothermic reaction in which GO loses ca. 30% of its original weight. Finally, the third step corresponds to the combustion of the carbonaceous solid until the total amount of carbon is oxidized to CO_2. No extra losses were detected for the GOFe samples that could have characterized the thermal behavior of the iron complex. It is due to the relatively low weight of the immobilized $Fe(bpy)_3^{2+}$ cations, and also their TG curve (not shown) has no steep weight loss steps. However, the presence of the complex can be seen from the (i) remnant weight above 600 °C and (ii) the deflagration temperatures. The remnant weight is <1.5 wt % for GO and GOFe4, indicating that GO is completely burned, while after the combustion of GOFe4 only a very low amount of iron oxide is retained. For the GOFe9 samples, the amount of residual iron oxide is higher (9−10 wt %). These are in fair agreement with the iron contents determined by ICP-AES. The deflagration temperatures (determined by ±2 °C accuracy) are found in Table 1. For pristine GO, τ = 275 °C, which fits in the range found for graphite oxides prepared by the Brodie method.[41] For the iron-exchanged samples, a significant decrease in the deflagration point was observed, and the higher the iron content was, the lower temperature τ dropped to. Boehm et al. showed that τ can be considerably lowered by impurities.[41] Here, we supplement this with the finding that the GOFe9 samples reach their constant weight at 100−150 °C lower temperatures than GO or GOFe4, indicating that, besides the decomposition of GO, the combustion speed of the carbon soot is also accelerated by the incorporation of the iron complex.

XRD of Iron Oxide/Carbon Composites. XRD patterns of solids obtained after calcination at 350 °C are shown in Figure 4. The diffractogram of GO soot is characterized by a single reflection with a *d*-spacing of 0.376 nm and a very large line breadth (Table 2), while in well-crystallized graphite d = 0.339 nm and the reflection is sharp. This suggests that an average carbon particle (L_c = 1.9 nm) is built up from only five graphenes, the basal planes of which are slipped sideways

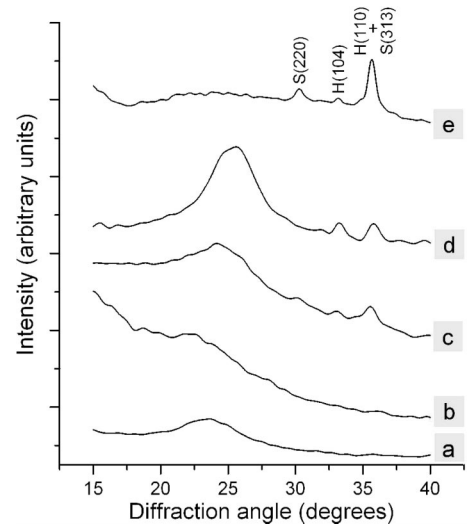

Figure 4. X-ray diffractograms of GO soot (a), CFe4-rap (b), CFe9-rap (c), CFe9-sl (d), and CFe9-rap calcined at 350 °C for 60 min (e). S and H with the Miller indices refer to the spinel type maghemite and the hematite phase, respectively.

TABLE 2: XRD Parameters, Iron(III) Oxide Contents, and Saturation Magnetizations of Graphite, GO Soot, and the Magnetic Carbon Samples

sample	2Θ°	d_{002} (nm)	L_c (nm)	N	Fe_2O_3 content (wt %)	M_S (emu/g)
graphite	26.28	0.339			0.0	
GO soot	23.60	0.376	1.9	5	0.0	
CFe4-sl	25.9	0.344	2.2	6	1.1	
CFe4-rap	22.36	0.398	1.9	5	0.9	
CFe9-sl	25.6	0.348	2.1	6	14	2.0
CFe9-rap	24.16	0.368	1.7	5	10.5	3.2

relative to each other, causing the spacing between the graphenes to be greater than in the ideal graphite lattice (turbostratic structure). The CFe-rap samples obtained after rapid heating (lines b and c) have basal spacings close to or even slightly higher than that of the GO soot. For the slowly heated samples (line d for CFe9-sl; not shown for CFe4-sl), the *d*-values are close to that of graphite. The reason is that the latter samples were kept at 350 °C for 30 min, during which the randomly stacked graphenes gradually ordered to graphitic carbon, while in the case of the "rap" samples the 5 min calcination was not enough for such transformation. On the other hand, the L_c and N values of the composites are the same as those measured for the GO soot, and are independent from the calcination time and heating rate. This means that the highly delaminated structure formed after the decomposition of GO is well preserved after the heat treatment, which is easily understood because the fusion of graphite crystallites along their layer planes requires higher activation energy than the ordering of graphenes inside a single crystallite.

Reflections of iron oxides or other phases were not detected in the diffractograms of CFe4 samples because they contain only 1 wt % Fe_2O_3. The presence of iron oxides in the CFe-9 composites containing >10 wt % "Fe_2O_3" are clearly seen in Figure 4 (lines c and d). In the case of a rapidly heated sample, reflections of both the rhombohedral hematite (α-Fe_2O_3) and the maghemite of spinel structure (γ-Fe_2O_3) are present, similarly to magnetically modified clays in our recent study.[42] When the carbon was completely burnt from the composite, the residue was magnetic due to the presence of maghemite. This phase was also found to dominate the residue by its XRD

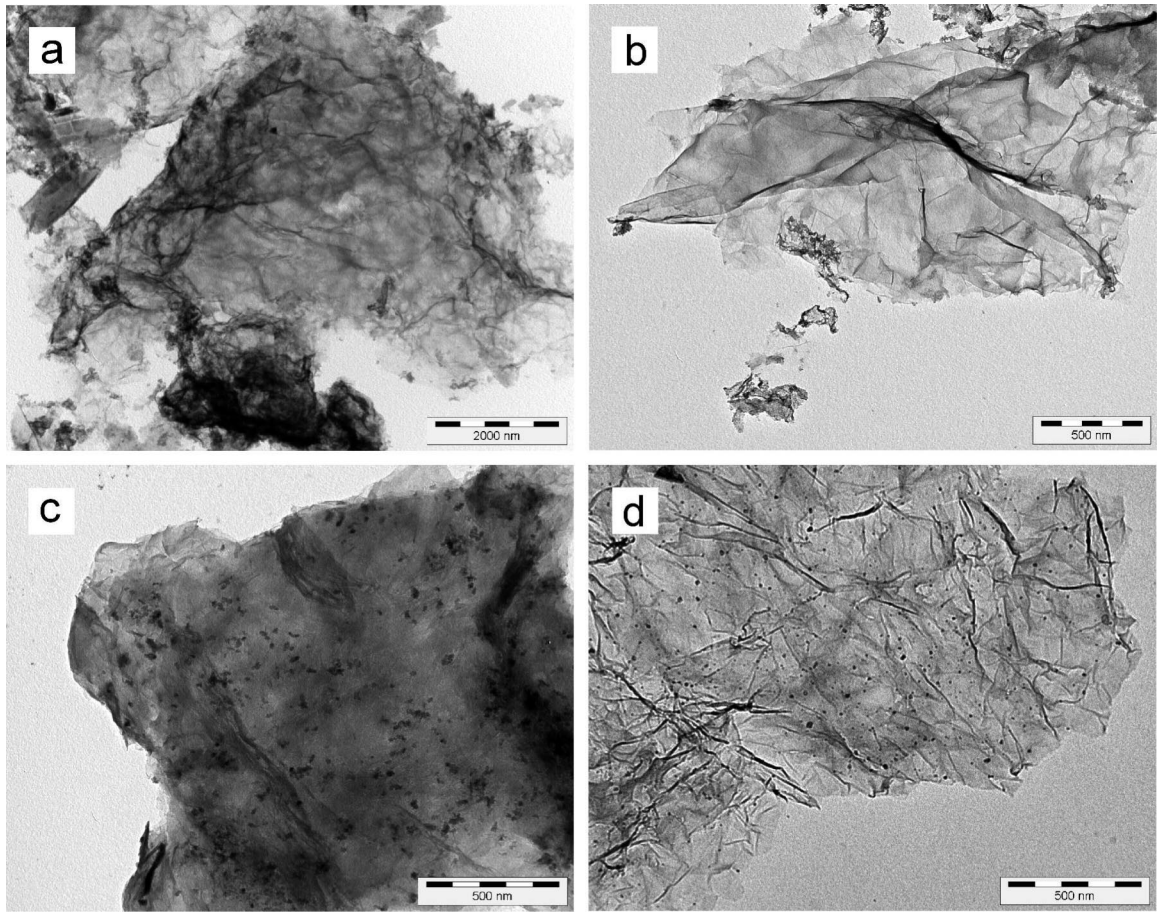

Figure 5. TEM images of GO soot (a), CFe4-rap (b), CFe9-sl (c), and CFe9-rap (d).

profile (line e). In contrast, the slowly heated sample gave no γ-Fe_2O_3 reflections. The much lower maghemite content of CFe9-sl suggests that either the formation of hematite is favored at slow heating rate or maghemite forms first but then it is recrystallized to hematite in 30 min. Finally, it is worth mentioning that the calcination product of the pure complex was not magnetic and its XRD pattern (not shown) does not feature iron(III) oxide reflections. Instead, it shows a large number of lines that are not useful for phase identification. Nevertheless, this signifies that $Fe(bpy)_3SO_4$ does not completely decompose at 350 °C to give Fe_2O_3.

Electron Microscopy. Figure 5 shows the TEM images of GO soot and the iron oxide/carbon nanocomposites. It is seen that the soot obtained from the deflagration of GO consists of large (lateral size of several micrometers) but very thin carbon flakes. These flakes have considerably rough surfaces, as found also in many other works for thermally treated or chemically reduced graphite oxides.[15–20] The wrinkling of the graphenes is attributed to point or line defects formed upon exfoliation or present in areas of a few intact epoxide groups.[40] The micrograph of the CFe4 sample features the same carbon foils with aggregated fine particles at a few locations around the edges of larger lamellae. Smaller foils may be completely covered, as seen at the bottom of the image. The surface of the CFe9 composites is decorated with a significantly higher number of hematite and maghemite nanocrystallites than that of CFe4. Size analysis showed that the diameter of the particles fell in the range 2−14 nm with an average size of 6 nm. The population of the smallest particles (d = 2−3 nm) was relatively large (15%), while particles with d > 12 nm were rarely found. CFe9-rap reveals the abundance of carbon foils, whose thickness is equal to those of elementary carbon layers.[15] Indeed, it has been recently found by atomic force microscopy that the thermally expanded GO may consist of up to 80% single graphene sheets.[20] Fe_2O_3 particles showed a perfectly homogeneous distribution over the graphene surface. Other micrographs of this sample displayed only a few aggregates or larger single particles. In the case of CFe9-sl, aggregates composed of several nanocrystals dominate in the composite, although individual Fe_2O_3 particles are still present. The other difference between the rapidly and slowly heated samples is that the carbon layer of the latter looks darker. At the upper part of Figure 6c, it is also apparent that thin lamellae are layered on underlying ones. These reflect the presence of particles built up from stacked graphenes in agreement with XRD results.

Vibrating Sample Magnetometry. The magnetization curves of the Fe_2O_3 loaded carbons are displayed in Figure 6. The shape for CFe9 samples displays zero coercive field and remanence. Thus, they are indicative of small, ferrimagnetic single domain particles of γ-Fe_2O_3 that behave as superparamagnetic entities. The presence of nanosized maghemite crystallites is in accordance with the electron microscopic analysis. The CFe9-rap sample has a higher saturation magnetization (M_S, Table 1) than that of CFe9-sl, despite its lower Fe_2O_3 content. This difference is even more remarkable if we compare M_S values related to the pure iron oxide phase, which are 14.3 and 30.5 emu/g for the CFe9-sl and CFe9-rap composites, respectively. Since the particle sizes (that would also modify the magnetic properties) are nearly identical for the solids, this result proves, along with XRD, that the maghemite/hematite ratio is larger in the rapidly heated composite. The magnetization curve of the CFe4 sample has a unique shape that shows the superposition

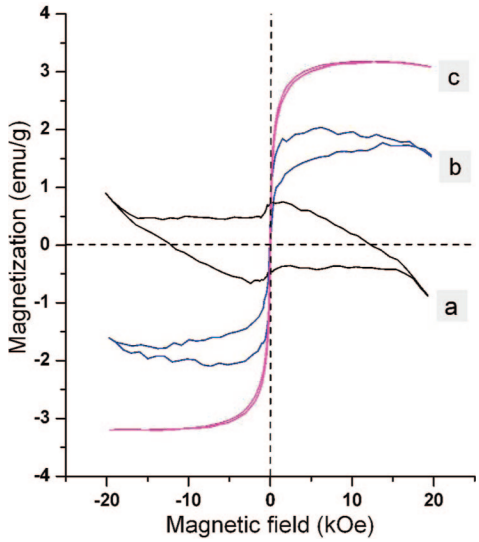

Figure 6. Magnetization curves of CFe4-rap (a), CFe9-sl (b), and CFe9-rap (c).

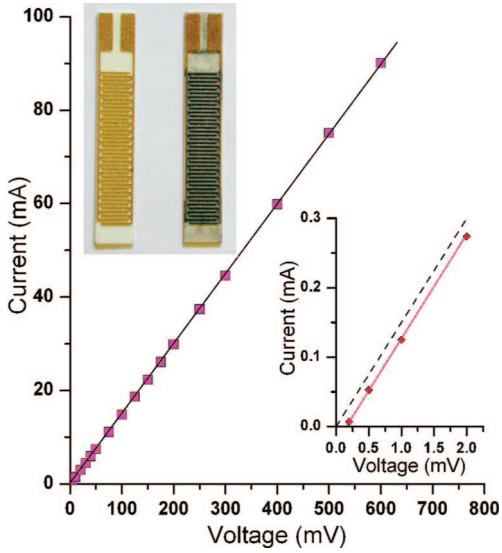

Figure 7. Current−voltage characteristic of CFe9-sl. The low voltage range of the characteristic (up to 2 mV) is enlarged in the inset (bottom right corner). The photograph in the top left corner shows the clean interdigitated gold electrode (on the left) and that covered by a thin film of CFe9-sl (on the right).

of a superparamagnetic and a diamagnetic component. The exceptionally large diamagnetic contribution arises from the pyrolytic carbon support, the susceptibility of which is suggested to be one of the largest for any diamagnet which is not a superconductor.[43] However, while the diamagnetic feature is still present on the magnetization curves of CFe9 samples, its contribution is less significant.

Electric Conductivity. The electric behavior of the CFe9 composite was tested on a sensor electrode displayed in the top inset of Figure 7. An aqueous suspension containing 16 mg of GOFe9 was cast on the 5 cm^2 surface of the interdigitated gold electrode. After the evaporation of water, a layer of GOFe9 adhered to the surface, which was found to be homogeneous by the naked eye. The average thickness of this layer is estimated to be 17 μm based on the true density of GOFe9 (1.9 g/cm^3) and assuming uniformity of thickness in nanometric dimensions. The GOFe9 coating could be easily peeled off as thin slabs from areas outside the electrode arrays,[44] showing that GOFe9 forms mechanically stiff, self-supporting membranes similar to those recently reported for pristine and divalent ion modified GO by Ruoff et al.[45,46] The GOFe9 film was an insulator because its resistance was higher than the maximum measurable value of the source meter ($R > 210$ MΩ). Clearly, the well oxidized GO is nonconductive and the immobilized $Fe(bpy)_3^{2+}$ ions cannot act as mobile charge carriers. In stark contrast, the film became conductive upon calcination, as seen from the current−voltage characteristics of the CFe9-sl film in Figure 7. The linear $I-V$ function indicates that the film obeys Ohm's law in a wide range of applied voltage with $R = 6.68$ Ω. The high (at least 31-million-fold) increase in the conductivity is explained by the transformation of the GO particles to a conductive graphitic film. The bottom inset of Figure 7 also shows that the current starts to flow above a threshold voltage of 0.2 mV. This is a low value that indicates only a slight hindrance for electron flow. This suggests that the particulate layer is well stuffed with direct contacts between the adjacent conductive particles or with very low interparticle distances.

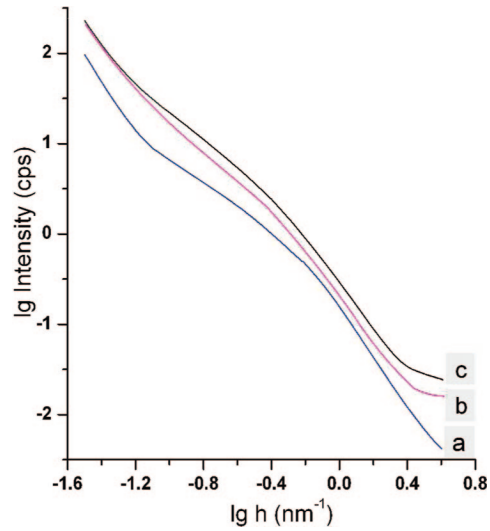

Figure 8. SAXS profiles of GO soot (a), CFe9-rap (b), and CFe9-sl (c).

TABLE 3: SAXS Parameters and Specific Surface Areas of the GO Soot and Its Magnetic Derivatives

sample	GO soot	CFe4-rap	CFe9-sl	CFe9-rap
D_s	2.10		2.38	2.45
l_S (nm)	3.3		8.2	4.1
l_C (nm)	6.4		15.2	7.7
a^s_{SAXS} (m^2/g)	640		260	510
a^s_{BET} (m^2/g)	800	920	230	450

Small-Angle X-ray Scattering and N_2 Adsorption. The scattering curves in logarithmic representation are shown in Figure 8 for GO soot and CFe9 samples, and Table 3 summarizes the derived structural parameters determined by calculations described earlier.[47] The shape of the scattering function is different for the GO soot and the magnetic CFe9 composites (the latter look very similar), which indicates that the nanostructure of the deflagration product of GO was changed by loading with Fe_2O_3. The surface fractal (D_s) of GO soot is 2.10, which means that the surface of the GO soot is not perfectly smooth in the nanometric dimensions. This is due to defects that generate crumpling of the layers as found by TEM. The fractal dimension is higher in both CFe9 samples, implying that the roughness of the surface increased upon decoration with Fe_2O_3 nanoparticles. The correlation lengths characterizing the average sizes of inhomogeneities in the solid/gas disperse system (l_C) and the statistical average size of the solid phase (l_S) reveal

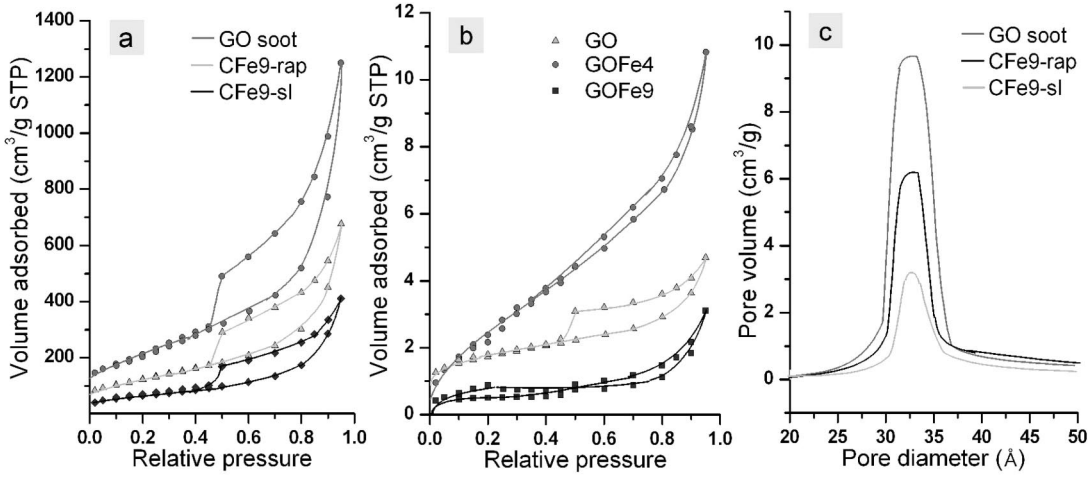

Figure 9. N_2 adsorption isotherms of the calcined samples (a), graphite oxide and ion-exchanged GOs (b), and the desorption pore volume plots of the calcined samples (c).

a highly delaminated and highly porous structure for all of the samples. The values of l_S fall in the range of the crystallite thicknesses (L_c) of the graphene support and the average diameters of the iron oxide nanoparticles. The l_C values are slightly larger, which is attributable to voids of several nm size between the composite particles filled with air. This is supported by N_2 adsorption measurements that gave type IV isotherms characteristic for mesoporous materials (Figure 9a). The characteristic pore diameters (Figure 9c) were ca. 33 nm for these samples, and the mesopore volumes were significantly higher (0.69, 1.06, and 1.95 cm^3/g for CFe9-sl, CFe9-rap, and GO soot, respectively) than those of GO (0.007 cm^3/g) and the ion-exchanged samples, which are nonporous. Finally, the specific surface areas determined by both N_2 adsorption (Figure 9a) and SAXS (Table 3) are much higher for all of the calcined solids than the parent or ion-exchanged graphite oxides (Table 1 and Figure 9b) and are in the range obtained for high-surface-area carbon adsorbents and graphite oxide-like foams.[48] Only CFe9-sl has a lower surface area in accordance with the higher correlation lengths. This is attributable to the onset of the fusion (crystallization) of graphitic particles.

Discussion

Utility of the $Fe(bpy)_3^{2+}$ Complex as an Iron Precursor. Preparation of a graphite oxide derivative with high and possibly uniform loading of iron species has prompted our effort to find a proper iron precursor. The starting point is that GO forms coarse particles consisting of many individual graphene oxide layers in slightly acidic (pH 4−5) aqueous suspensions. Impregnation of GO is not useful at these original, acidic conditions because dissolved species may only deposit on the external surfaces of these particles. The interlamellar space becomes accessible for iron precursors only at higher pHs (8−10), where GO exfoliates. Thus, the application of simple Fe(II) or Fe(III) salts fails because their fast hydrolysis at alkaline pHs results in uncontrollable aggregation/precipitation of the formed oxyhydroxide particles. However, the application of tris(2,2′-bipyridyl) iron(II) ions as an iron precursor offers the following advantages:

(1) The complex has a very high stability constant, so it is protected from hydrolysis even at alkaline pHs.

(2) The bipyridine ligands are neutral. Thus, the complex is positively charged and can undergo cation-exchange reactions.

(3) The chelation of the iron species by a proper complexant is suggested to promote the formation of magnetic iron oxide phases.[9]

Structure and Adsorption Mechanism of the $Fe(bpy)_3^{2+}$ Loaded Graphite Oxides. The very low iron content and low basal spacings of GOFe samples prepared at pH 4 point out that the precursor is adsorbed only on the external surfaces of the graphite oxide particles. Direct intercalation of the large complex ions is not possible. For the adsorption of a significant amount of $Fe(bpy)_3^{2+}$, the GO particles must be delaminated first in a dilute basic solution. The as-formed individual graphene oxide sheets are then restacked due to the electrostatic interactions between the negatively charged GO surfaces and the divalent complex ions. Washing of the solid with water decreases the pH with the concomitant decrease of negatively charged sites. These surface sites progressively release the iron precursor, which means that the following ion-exchange reaction takes place:

$$2Na^+(H_2O)_n{-}GO + Fe(bpy)_3^{2+} \rightarrow GO{-}Fe(bpy)_3^{2+}{-}GO + 2Na^+(H_2O)_n \quad (1)$$

This reaction must tend strongly to the right because divalent ions have higher affinity toward oppositely charged surfaces than monovalent Na^+ (lyotropic sequence). Restacking of GO platelets is induced by the divalent $Fe(bpy)_3^{2+}$ that make connection between two GO sheets. The original crystallite thickness is not restored after restacking, as seen from the abrupt decrease of the average number of graphenes from 35 (in GO) to 5 (GOFe9). The large sediment volume of GOFe9 also suggests a more opened structure with "incomplete" restacking.

The interlayer distance (0.64 nm) is lower than the calculated diameter of the intercalant complex (1.17 nm), whose structure is shown in Figure 10. The distance between the opposite N donor atoms in the octahedral coordination sphere of the iron center is equal to 0.394 nm. This is the lowest possible value to explain an intercalation reaction between the complex ion and graphite oxide. Clearly, the interlayer is large enough to accommodate the $Fe(bpy)_3^{2+}$ ions, but the complex is obviously not in the same conformation in the confined nanospace as the ideal "spherical" structure that the complex adopts in solution, as shown in Figure 10. It can be envisioned that the bipyridine ligands or even the octahedral coordination sphere of the iron center is squeezed in the interlayer of GO due to the considerable adhesion forces acting between the planar graphene oxide surfaces. Further investigation would certainly be necessary to confirm the changes in the spatial structure of $Fe(bpy)_3^{2+}$, but this leads beyond the subject of the present publication.

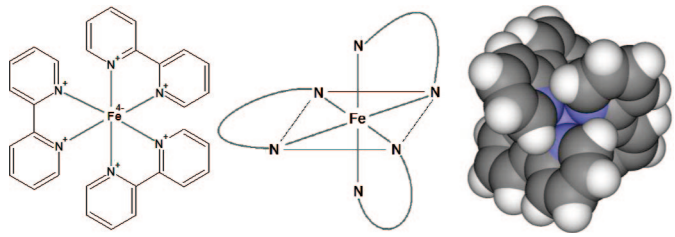

Figure 10. (left) Chemical structure of the homoleptic $Fe(bpy)_3^{2+}$ complex. (middle) Octahedral geometry with a distance between opposite N donors of 0.394 nm. (right) 3D view of the complex. The calculated diameter of this structure is 1.17 nm.

The quantitative comparison of the $Fe(bpy)_3^{2+}$ content and the surface charging curve of graphite oxide show that the adsorbed amount of the complex is similar to the actual cation-exchange capacity of the support (both in mmol/g). However, according to reaction 1, the divalent $Fe(bpy)_3^{2+}$ occupies two monovalent ion-exchange positions. Thus, they cannot be immobilized electrostatically by the available negatively charged sites, which means that the precursor can be bound with mechanisms other than ion exchange. Ligand-exchange reaction involving the replacement of bpy by the surface functional groups of GO (carboxylate, phenolate) or dispersion interactions between the aromatic bpy and the unoxidized regions of GO may be possible.

Structure and Properties of Iron Oxide/Carbon Composites. Thermoanalytical investigations of the ion loaded graphite oxides show that the calcination temperature must be chosen carefully. GO does not decompose to conductive and high-surface-area graphenes below 200 °C. Temperatures higher than 350−400 °C should also be avoided because the complex catalyzes the ignition of the carbon. Although the carbon support could be preserved at higher temperatures using an inert atmosphere or vacuum, the lack of oxygen would prevent the combustion of the complex and thus the formation of Fe_2O_3. Unlike pure $Fe(bpy)_3SO_4$, the GOFe9 samples form iron oxides upon calcination. This must be due to the higher susceptibility of the distorted complex toward thermal degradation. The heating rate was also found to influence the nanostructure and properties of the composites. The sample obtained after a rapid heat treatment and vigorous thermal expansion is composed of very thin carbon lamellae with high surface area. Only several, turbostratic stacked carbon sheets constitute these particles, although single graphenes can also be observed by TEM. The large, rough surfaces are covered homogeneously by ultrafine maghemite particles that exhibit superparamagnetic properties. Upon prolonged exposure to higher temperature after slow heating, both the iron oxide nanocrystals and the carbon support are aggregated, which results in lower specific surface area. Such treatment is disadvantageous also because it favors the formation of antiferromagnetic hematite at the expense of superparamagnetic maghemite.

Conclusions

Superparamagnetic iron oxide nanoparticles can be successfully prepared on single or turbostratic stacked graphenes, that constitute an electrically conductive matrix with high surface area. The strategy of this solution-based synthesis relies on the adsorption of large amounts of a divalent iron(II) chelate complex on the high surface of exfoliated GO sheets under slightly alkaline conditions. The complex ions are intercalated between the GO in a different conformation as compared to that adopted in solution. This distorted structure or the high exothermity of the deflagration of GO can be accounted for by the easier thermal decomposition and formation of a magnetic iron oxide phase, which is not generated when the pure complex is treated under identical conditions. The present composite may be a good candidate as an adsorption material for magnetic separation or an alternative of magnetic carbon materials prepared by standard physical methods such as the electric arc technique or cosputtering.

Acknowledgment. The present publication was supported by the Innovation Fund of Science and Research (Hungary) and the General Secretariat for Research and Technology (Greece) in the frame of a Greek-Hungarian Intergovernmental Science & Technology cooperation.

References and Notes

(1) Cornell, R. M.; Schwertmann, U. *The Iron Oxides*; WILEY-VCH: Weinheim, Germany, 1996.
(2) Roger, J.; Pons, J. N.; Massart, R.; Halbreich, A. J.; Bacri, C. *Eur. Phys. J. Appl. Phys.* **1999**, *5*, 321.
(3) Sun, S.; Murray, C. B.; Weller, D.; Folks, L.; Moser, A. *Science* **2000**, *287*, 1989.
(4) Bourlinos, A. B.; Karakassides, M. A.; Simopoulos, A.; Petridis, D. *Chem. Mater.* **2000**, *12*, 2640.
(5) Tombácz, E.; Libor, Z.; Illés, E.; Majzik, A.; Klumpp, E. *Org. Geochem.* **2004**, *35*, 257.
(6) Galindo-González, C.; de Vincente, J.; Ramos-Tejada, M. M.; López-López, M. T.; González-Caballero, F.; Durán, J. D. G. *Langmuir* **2005**, *21*, 4410.
(7) Bourlinos, A.; Simopoulos, A.; Petridis, D.; Okumura, H.; Hadjipanayis, G. *Adv. Mater.* **2001**, *13*, 289.
(8) Tartaj, P.; González-Carreño, T.; Serna, C. J. *J. Phys. Chem. B* **2003**, *107*, 20.
(9) Bourlinos, A. B.; Zboril, R.; Petridis, D. *Microporous Mesoporous Mater.* **2003**, *58*, 155.
(10) Jang, J.; Yoon, H. *Adv. Mater.* **2003**, *15*, 2088.
(11) Morigishe, K.; Hamada, T. *Langmuir* **2005**, *21*, 6277.
(12) Zou, Y.-H.; Liu, H.-B.; Yang, L.; Chen, Z.-Z. *J. Magn. Magn. Mater.* **2006**, *302*, 343.
(13) Hung, C. C. *Carbon* **1995**, *33*, 315.
(14) Li, D.; Müller, M. B.; Gilje, S.; Kaner, R. B.; Wallace, G. G. *Nat. Nanotechnol.* **2008**, *3*, 101.
(15) Boehm, H.-P.; Clauss, A.; Fischer, G. O.; Hofmann, U. *Z. Naturforsch.* **1962**, *17*, 150.
(16) Bourlinos, A. B.; Gournis, D.; Petridis, D.; Szabó, T.; Szeri, A.; Dékány, I. *Langmuir* **2003**, *19*, 6050.
(17) Szabó, T.; Szeri, A.; Dékány, I. *Carbon* **2005**, *43*, 87.
(18) Stankovich, S.; Piner, R. D.; Chen, X.; Wu, N.; Nguyen, S. T.; Ruoff, R. S. *J. Mater. Chem.* **2006**, *16*, 155.
(19) Gómez-Navarro, C.; Weitz, R. T.; Bittner, A. M.; Scolari, M.; Mews, A.; Burghard, M.; Kern, K. *Nano Lett.* **2007**, *7*, 3499.
(20) McAllister, M. J.; Li, J.-L.; Adamson, D. H.; Schniepp, H. C.; Abdala, A. A.; Liu, J.; Herrera-Alonso, M.; Milius, D. L.; Car, R.; Prud'homme, R. K.; Aksay, I. A. *Chem. Mater.* **2007**, *19*, 4396.
(21) Dékány, I.; Krüger-Grasser, R.; Weiss, A. *Colloid Polym. Sci.* **1998**, *276*, 570.
(22) Matsuo, Y.; Hatase, K.; Sugie, Y. *Chem. Mater.* **1998**, *10*, 2266.
(23) Matsuo, Y.; Niwa, T.; Sugie, Y. *Carbon* **1999**, *37*, 897.
(24) Matsuo, Y.; Tabata, T.; Fukunaga, T.; Fukutsuka, T.; Sugie, Y. *Carbon* **2005**, *43*, 2875.
(25) Matsuo, Y.; Miyabe, T.; Fukutsuka, T.; Sugie, Y. *Carbon* **2007**, *45*, 1005.
(26) Seredych, M.; Pietrzak, R.; Bandosz, T. J. *Ind. Eng. Chem. Res.* **2007**, *46*, 6925.
(27) Du, X. S.; Yu, Z.-Z.; Dasari, A.; Ma, J.; Mo, M.; Meng, Y.; Mai, Y.-W. *Chem. Mater.* **2008**, *20*, 2066.

(28) Lerf, A.; He, H.; Forster, M.; Klinowski, J. *J. Phys. Chem. B* **1998**, *102*, 4477.

(29) Szabó, T.; Berkesi, O.; Forgó, P.; Josepovits, K.; Sanakis, Y.; Petridis, D.; Dékány, I. *Chem. Mater.* **2006**, *18*, 2740.

(30) Slabaugh, W. H.; Seiler, B. C. *J. Phys. Chem.* **1962**, *66*, 396.

(31) Seredych, M.; Bandosz, T. J. *J. Phys. Chem. C* **2007**, *111*, 15596.

(32) Szabó, T.; Tombácz, E.; Illés, E.; Dékány, I. *Carbon* **2006**, *44*, 537.

(33) Hirata, M.; Gotou, T.; Ohba, M. *Carbon* **2005**, *43*, 503.

(34) Watcharotone, S.; Dikin, D. A.; Stankovich, S.; Piner, R.; Jung, I.; Dommett, G. H. B.; Evmenenko, G.; Wu, S.-E.; Chen, S.-F.; Liu, C.-P.; Nguyen, S. T.; Ruoff, R. S. *Nano Lett.* **2007**, *7*, 1888.

(35) Gilje, S.; Han, S.; Wang, M.; Wang, K. L.; Kaner, R. B. *Nano Lett.* **2007**, *7*, 3394.

(36) Becerril, H. A.; Mao, J.; Liu, Z.; Stoltenberg, R. M.; Bao, Z.; Chen, Y. *ACS Nano* **2008**, *2*, 463.

(37) Brodie, B. *Ann. Chim. Phys.* **1855**, *45*, 351.

(38) Lerf, A.; Buchsteiner, A.; Pieper, J.; Schöttl, S.; Dékány, I.; Szabó, T.; Boehm, H.-P. *J. Phys. Chem. Solids* **2006**, *67*, 1106.

(39) Paci, J. T.; Belytschko, T.; Schatz, G. C. *J. Phys. Chem. C* **2007**, *111*, 18099.

(40) Schniepp, H. C.; Li, J.-L.; McAllister, M. J.; Sai, H.; Herrera-Alonso, M.; Adamson, D. H.; Prud'homme, R. K.; Car, R.; Saville, D. A.; Aksay, I. A. *J. Phys. Chem. B* **2006**, *110*, 8535.

(41) Boehm, H.-P.; Scholz, W. *Z. Anorg. Allg. Chem.* **1965**, *335*, 74.

(42) Szabó, T.; Bakandritsos, A.; Tzitzios, V.; Papp, S.; Korosi, L.; Galbács, G.; Musabekov, K.; Bolatova, D.; Petridis, D.; Dékány, I. *Nanotechnology* **2007**, *18*, 285602.

(43) Stamenov, P.; Coey, J. M. D. *J. Magn. Magn. Mater.* **2005**, *290*−*291*, 279.

(44) It is necessary to remove the GOFe9 coating from the vicinity of the two wide wires at the top of the electrode to avoid a possible shortcut for conductive samples.

(45) Dikin, D. A.; Stankovich, S.; Zimney, E. J.; Piner, R. D.; Dommett, G. H. B.; Evmenenko, G.; Nguyen, S. T.; Ruoff, R. S. *Nature* **2007**, *448*, 457.

(46) Park, S.; Lee, K.; Bozoklu, G.; Cai, W.; Nguyen, S. T.; Ruoff, R. S. *ACS Nano* **2008**, *2*, 572.

(47) Dékány, I.; Turi, L. *Colloids Surf., A* **1997**, *126*, 59.

(48) Bourlinos, A. B.; Steriotis, T. A.; Karakassides, M.; Sanakis, Y.; Tzitzios, V.; Trapalis, C.; Kouvelos, E.; Stubos, A. *Carbon* **2007**, *45*, 852.

JP802879A